

chroton by the iron and concrete wall. The intensity of the bremsstrahlung was monitored by a thick-faced aluminum chamber which had been calibrated relative to a standard P2 Chamber.¹⁰

The bremsstrahlung beam was collimated so the sample was irradiated within a central section 3.5 cm in diameter. The collimator axis and center-line position of the beam were coincident to within ± 0.03 cm at either end of the collimator and parallel to less than 0.002 rad. The angular change in center-line direction with energy was less than ± 0.0005 rad for energies between 20 and 60 MeV.

Yield points were taken every 0.5 MeV from below threshold to 65 MeV. A yield curve was composed of one such series of yield points. Six separate yield curves were obtained using the silicon sample and six for the aluminum sample.

While accumulating data for a single yield point the detection equipment and the synchrotron were run through 50 irradiation and counting cycles. After a bombardment period of duration t_b , a 50-msec delay time t_d elapsed. The sample activity was then counted for a time t_c . During the irradiation interval the detector output pulses were blocked. During the counting interval, electron injection into the synchrotron was blocked.

The data were accumulated in a multichannel analyzer operated in the 8×128 configuration. During the counting period a time sequence of eight spectra were obtained. A pulse from one of the NaI(Tl) detectors was accepted for analysis only if it was in coincidence

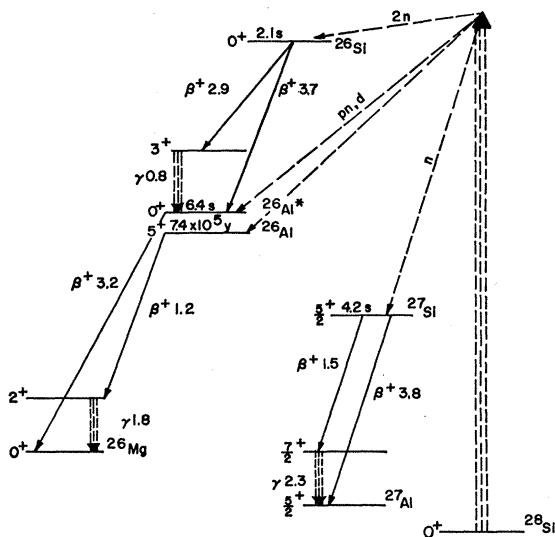


FIG. 2. The decay scheme for the major photoreaction products from Si^{28} . The information is taken from Ref. 11. Since Si^{26} decays via positron emission to Al^{26*} which is also positron active, the yield due to production of Si^{26} is enhanced relative to the yield due to formation of Si^{27} .

¹⁰ J. S. Pruitt and S. R. Domen, Natl. Bur. Std. Monograph 48 (1962).

TABLE I. Peak energies for the cross-section maxima of Figs. 4 and 5. All maxima with greater than 70% likelihood as computed from the cross-section errors^a are shown. Maxima with less than 90% likelihood are doubtful.

Al^{27}		Si^{28}	
Energy (MeV)	Likelihood	Energy (MeV)	Likelihood
41.6 ± 1.0	0.72	27.1 ± 0.5	0.90
49.4 ± 0.8	0.96	31.4 ± 0.4	0.88
56.3 ± 0.9	0.98	3.47 ± 0.6	0.86
		40.1 ± 0.9	0.89
		46.4 ± 0.8	1.00
		52.2 ± 0.8	1.00
		58.2 ± 1.0	0.98

^a B. C. Cook (to be published).

($T_R = 0.5 \mu\text{sec}$) with a pulse from the other detector. The spectra were dominated by the 0.511-MeV annihilation line.

The mode of operation is defined $t_b \times (t_d + t_c)$ in seconds. For the aluminum data the mode used was 12×24 and for silicon the mode was 8×15 . During an irradiation period for silicon some of the Si^{26} nuclei formed will decay into Al^{26*} . This indirect production of Al^{26*} will contribute to the experimental yield. During the counting period many of the Si^{26} nuclei present will decay through Al^{26*} to Mg^{26} with the emission of two positrons. Thus the probability for detection of a decay event related to the production of Si^{26} is enhanced compared to the probability for detection of a Si^{27} decay event. The enhancement factor can be calculated from the half-lives and the times t_b and t_c . This enhancement is indicated when the results are discussed.

The data were analyzed with the Iowa State IBM 360/50 computer. The data taken from the memory of the multichannel analyzer were corrected for gain fluctuations in the detectors and for dead-time losses. For each yield point a decay curve was determined from the data taken in the eight successive time intervals. Using a minimum χ^2 procedure the contribution due to activities with $T_{1/2} \gg 1$ sec was subtracted from the major activity. The decay constant for the major activities was also obtained. For data points taken at energies below 24.0 MeV the half-life was measured as $T_{1/2} = 6.36 \pm 0.06$ sec for the aluminum data. This half-life is characteristic of Al^{26*} . The half-life time for Si^{27} was measured as $T_{1/2} = 4.16 \pm 0.04$ sec from silicon data taken at energies below 26.0 MeV. The agreement with half-life previously published^{11,12} for Al^{26*} and Si^{27} is within the errors. The yield curve obtained by averaging the individual yield points for aluminum had an average standard deviation of less than $\pm 0.30\%$ for points

¹¹ P. M. Endt and C. Van der Dornen, Nucl. Phys. 34, 1 (1962).

¹² J. M. Freeman, J. H. Montague, G. Murray, and R. E. White, Nucl. Phys. 69, 433 (1965).

SHIELDING FOR DETECTORS

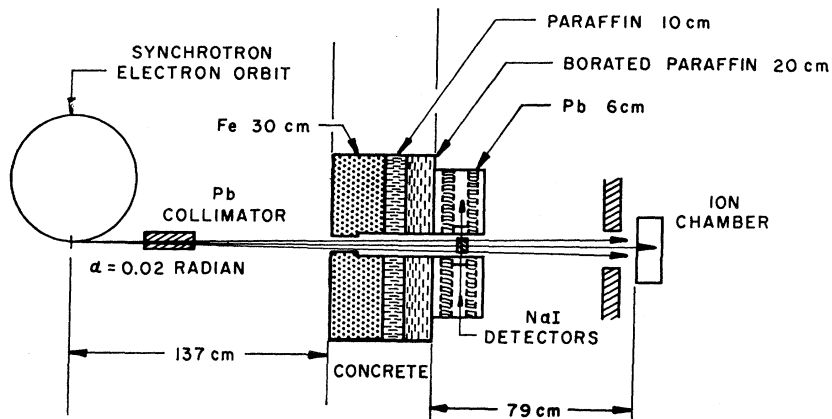


FIG. 3. The experimental arrangement. The synchrotron electron orbit is represented to the left. The bremsstrahlung beam is incident upon the sample which is held between the scintillation detectors. The ion chamber monitors the intensity of the bremsstrahlung.

above 35.0 MeV. The average standard deviation for the silicon yield points was less than $\pm 0.27\%$ for points above 26.0 MeV.

III. RESULTS AND TESTS

The least structure method⁷ for obtaining cross section from bremsstrahlung activation curves was utilized in the analysis. The least-structure solution reduces to the Penfold-Leiss solution¹³ when no smoothing is applied. However, smoothing is necessary to eliminate spurious cross-section oscillations at energies above the giant resonance when bremsstrahlung yields are analyzed. The amount of smoothing applied is determined by the standard deviation of the yield points in the least-structure procedure. The smoothing decreases the experimental resolution since the neighboring cross-section points are correlated.

The least-structure cross-section solutions for aluminum and silicon are shown in Figs. 4 and 5, respectively.

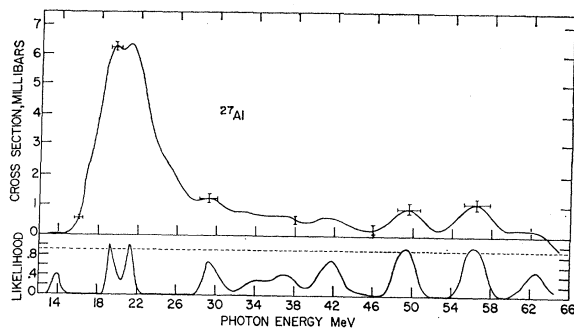


FIG. 4. The least-structure cross-section solution, $\sigma = \sigma_n + 0.9\sigma_{2n}$, for aluminum. Vertical bars indicate errors in cross section. The experimental timing was such that the contribution due to the reaction $Al^{27}(\gamma, 2n)Al^{25}$ was depressed relative to the contribution due to the $Al^{27}(\gamma, n)Al^{26*}$ reaction. A likelihood estimate of the statistical certainty of the indicated structure is also shown.

¹³ A. S. Penfold and J. E. Leiss, Phys. Rev. **114**, 1332 (1959).

The vertical bars represent cross-section errors and the horizontal bars indicate the width of the resolution function or the interval of high correlation for the cross-section points. Maxima in the curve indicate energy regions where the average cross section is large and any maximum may contain several resonances smoothed together.

Three individual least-structure cross-section curves for aluminum are shown in Fig. 6. They were obtained from yield curves generated after subdividing the data into three groups. The curves are undersmoothed. This figure indicates that the cross-section maxima which appear in the average cross section also occur in each of the individual cross-section curves. Thus the effect of statistical fluctuations in the yield is not significant for least structure solutions.

Figure 7 illustrates the effect on the reduced yield when several cross-section maxima are removed by arbitrarily setting the cross section equal to zero. The reduced yield curves shown in the inset were obtained from cross sections A, B, and C. The A is the aluminum

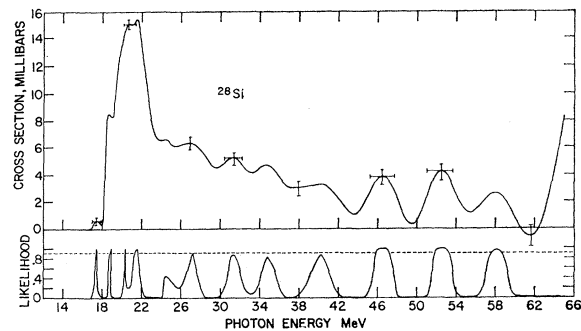


FIG. 5. The least-structure cross section, $\sigma = \sigma_n + 2.0\sigma_{2n} + \sigma_{pn*}$, for the silicon data. Vertical bars indicate errors in cross section. Horizontal bars indicate the resolution function width. The coefficient for σ_{2n} arises because of enhancement of the yield due to formation of Si^{26} as discussed in Sec. II. A likelihood estimate of the statistical certainty of the indicated structure is also shown.

cross section. Some of the experimental yield points are also plotted. The errors on the experimental points are considerably smaller than the distortions necessary to remove the high-energy cross section.

Table I gives the peak energies for maxima above the giant resonance for both the aluminum and the silicon curves. Figures 8 and 9 show the integrated cross sections for the aluminum and silicon reactions as a function of energy. The aluminum and silicon relative cross sections were put into absolute units using the appropriate averages from the results of measurements previously reported.^{1,14-18}

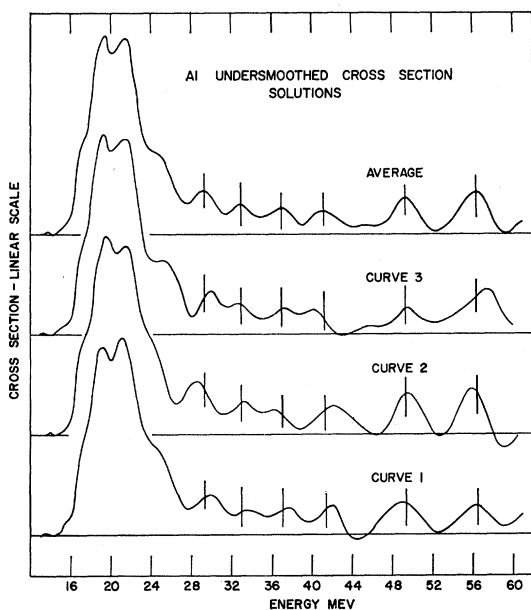


FIG. 6. A comparison of undersmoothed aluminum cross sections for the individual curves and the average.

IV. DISCUSSION

The cross-section determinations cited in Refs. 1-3 cover the giant resonance region of Al^{27} and Si^{28} in detail. The present experiment offers no new information in this region. However, no measurements with comparable resolution have been reported for Al^{27} and Si^{28} cross sections above 30 MeV.

The total photoneutron cross section of Al^{27} was measured by Fultz *et al.*² to a maximum energy of 37 MeV. Their results are not directly comparable to the aluminum cross section shown in Fig. 4 because of

¹⁴ F. Ferrero, R. Malvano, S. Menardi, and O. Terracini, Nucl. Phys. **9**, 32 (1958).

¹⁵ R. N. H. Haslam, W. Roberts, and P. Robb, Can. J. Phys. **32**, 351 (1954).

¹⁶ L. Katz and A. G. W. Cameron, Phys. Rev. **84**, 1115 (1951).

¹⁷ R. G. Summer-Gill, R. N. H. Haslam, and L. Katz, Can. J. Phys. **31**, 70 (1953).

¹⁸ L. Katz, R. N. H. Haslam, J. Goldenberg, and J. G. V. Taylor, Can. J. Phys. **32**, 580 (1954).

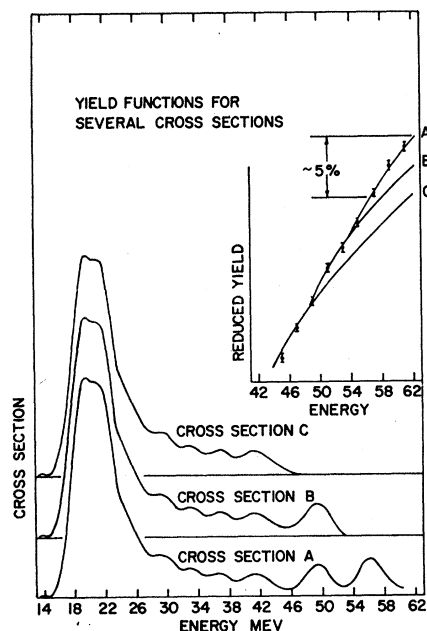


FIG. 7. Cross-section distortions. The inset yield curves A, B, and C which were calculated from cross sections A, B, and C, respectively. Some of the experimental yield points are also shown. The errors on experimental points are considerably smaller than the yield distortions necessary to remove high-energy cross-section maxima.

dominating contributions due to the $\text{Al}^{27}(\gamma, n)\text{Al}^{26g}$ and the $\text{Al}^{27}(\gamma, pn)\text{Mg}^{25}$ reactions. The $\text{Al}^{27}(\gamma, 2n)\text{Al}^{25}$ reaction was separated from other reactions in the work of Fultz *et al.*² and was found to increase with energy from zero at 24.5 MeV to approximately 1 mb at 37 MeV. These results indicate that the aluminum cross section shown in Fig. 4 must be largely due to the reac-

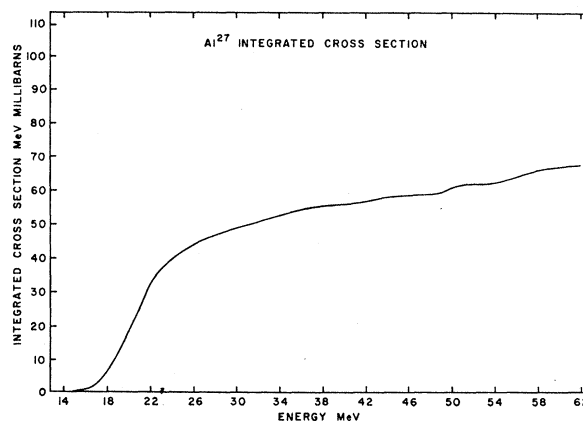


FIG. 8. Al^{27} integrated cross section as a function of energy. The absolute cross section was not measured calibration points for the relative cross section were taken from Refs. 1, 14, and 15. The quantity shown is

$$\bar{\sigma} = \int_0^E (\sigma_n + 0.9\sigma_{2n}) dE.$$

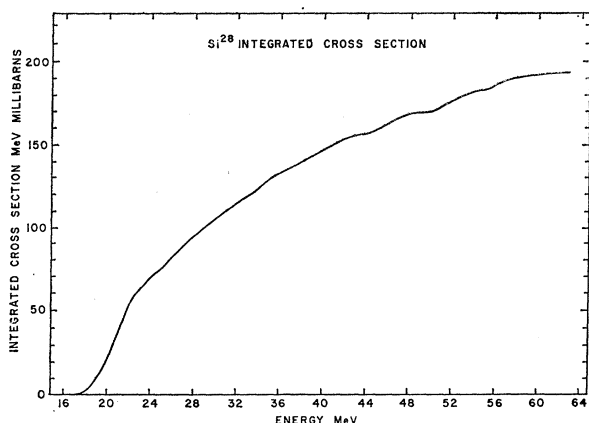


FIG. 9. The integrated cross section for Si^{28} . Calibration points for the relative cross section were taken from Refs. 16, 17, and 18. The function illustrated is

$$\bar{\sigma} = \int_0^E (\sigma_n + 2.0\sigma_{2n} + \sigma_{pn}) dE.$$

tion liberating two neutrons in the energy region between 30 and 40 MeV at least.

The integrated cross sections for the 46.4-, 52.5-, and 58.2-MeV silicon cross-section maxima are approximately 13, 13, and 9 MeV mb, respectively. The integrated cross sections for the 49.4- and 56.3-MeV maxima in the aluminum cross section are approximately 4 and 5 MeV mb, respectively. The difference in size between the aluminum and silicon maxima may be partially due to the increased probability for counting the Si^{26} decay events as discussed in Sec. III. This is particularly true if the $\text{Si}^{28}(\gamma, 2n)\text{Si}^{26}$ reaction is dominant in this region.

The average cross section in the region from 25 to 40 MeV is relatively large for silicon when compared to the aluminum results. A major part of the silicon cross section in this region is presumably due to the $\text{Si}^{28}(\gamma, pn)\text{Al}^{26*}$ reaction. The cross section for the

comparable reaction in S^{32} is known to peak in this region with a maximum cross section of 4.2 mb.¹⁹

Dependence of the giant resonance peak energy on $A^{-1/3}$ has been noted by several authors^{20,21} and is assumed for the shell-model spacing of harmonic oscillator levels.²² Al^{27} and Si^{28} have nearly the same values of $A^{-1/3}$. Thus one might expect corresponding cross-section maxima to fall at the same energies in aluminum and silicon.

Although the giant resonance peak energies are nearly comparable for the aluminum and silicon cross sections, the distinct maxima occurring above 45 MeV for aluminum have peak energies about ± 3 MeV from those for silicon. Thus a slow dependence such as $A^{-1/3}$ is not indicated here. A more detailed description of the nuclear level spacing is required for an explanation of individual energies of maxima.

The positions of the high-energy peaks have been shown to correlate well with peak positions in other $2s-1d$ nuclei.²³ More precisely, a family of peaks were found, the energy of which forms a linear function of mass number A . One of the lines followed the position of the $1s$ level as determined experimentally in $(e, e'p)$ experiments. Thus the peaks above 50 MeV are probably photoexcitations of $(1s)$ nucleons to the particle continuum. The position of the $1s$ level has been predicted to lie at 59.6 MeV in Si^{28} by Elton and Swift.²⁴ This should correspond to the peak found in our data at 58.2 ± 1.0 MeV for this peak is on the line corresponding to the $(1s)$ level position. The agreement is quite satisfactory.

¹⁹ L. Bonazzola, O. Borello, S. Costa, and S. Ferroni, Nucl. Phys. **34**, 637 (1962).

²⁰ M. Danos, Ann. Physik **10**, 265 (1952).

²¹ J. H. Carver, D. C. Peasley, and R. B. Taylor, Phys. Rev. **120**, 2155 (1960).

²² S. G. Nilsson, Kgl. Danske Videnskab. Selskab, Mat.-Fys. Medd. **29**, 16 (1955).

²³ B. C. Cook, D. W. Anderson, and T. J. Englert, Phys. Letters **26B**, 341 (1968).

²⁴ L. R. B. Elton and A. Swift, Nucl. Phys. **A94**, 52 (1967).